
Attention-Driven Hierarchical Reinforcement Learning with Particle Filtering for Source Localization in Dynamic Fields

Yiwei Shi¹*, Mengyue Yang¹, Qi Zhang³, Weinan Zhang², Cunjia Liu⁴, Weiru Liu¹

¹ School of Engineering Mathematics and Technology, University of Bristol

² Department of Computer Science & Engineering, Shanghai Jiao Tong University

³ School of Electronic and Information Engineering, Tongji University

⁴ Department of Aeronautical and Automotive Engineering, Loughborough University

{yiwei.shi, mengyue.yang, weiru.liu}@bristol.ac.uk

zhangqi_cs@tongji.edu.cn, c.liu5@lboro.ac.uk, wnzhang@sjtu.edu.cn

Abstract

In many real-world scenarios, such as gas leak detection or environmental pollutant tracking, solving the Inverse Source Localization and Characterization problem involves navigating complex, dynamic fields with sparse and noisy observations. Traditional methods face significant challenges, including partial observability, temporal and spatial dynamics, out-of-distribution generalization, and reward sparsity. To address these issues, we propose a hierarchical framework that integrates Bayesian inference and reinforcement learning. The framework leverages an attention-enhanced particle filtering mechanism for efficient and accurate belief updates, and incorporates two complementary execution strategies: Attention Particle Filtering Planning and Attention Particle Filtering Reinforcement Learning. These approaches optimize exploration and adaptation under uncertainty. Theoretical analysis proves the convergence of the attention-enhanced particle filter, while extensive experiments across diverse scenarios validate the framework's superior accuracy, adaptability, and computational efficiency. Our results highlight the framework's potential for broad applications in dynamic field estimation tasks.

1 Introduction

Many real-world problems, such as locating a gas leak in an industrial plant, detecting an electromagnetic anomaly in a power grid, or identifying a pollution source in a water body, involve navigating dynamic field distributions—spatially and temporally varying fields shaped by complex environmental interactions. Solving these problems is critical for ensuring safety, minimizing environmental damage, and maintaining system integrity. A prominent and technically demanding instance of such problems is the Inverse Source Localization and Characterization (ISLC) problem Steiner & Bushe (2001). The ISLC problem involves inferring the location, magnitude, and temporal characteristics of an unknown source within a complex field, based on sparse, noisy, and localized observations. This problem is ubiquitous in high-stakes applications such as gas leak detection, nuclear accident response, and environmental pollutant tracking, where accurate estimation of source parameters is crucial for effective mitigation and intervention.

However, solving the ISLC problem poses significant challenges due to the complex and uncertain nature of dynamic fields. First, partial observability is a fundamental obstacle, as measurements

*

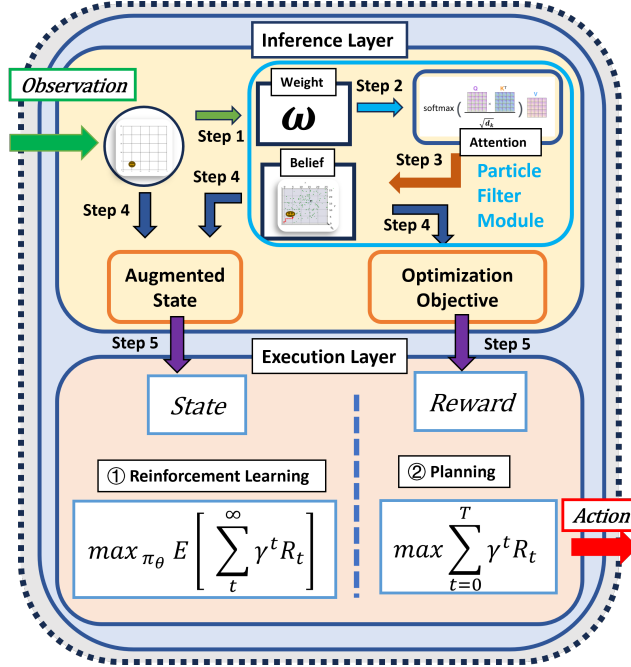


Figure 1: Hierarchical Attention-Based Inference Framework

(e.g., gas concentration, electromagnetic field strength) are often sparse, noisy, and localized, providing only limited insight into the underlying field distribution. Second, the temporal and spatial dynamics of these fields—shaped by environmental factors such as wind, interference, or source movement—result in constantly evolving conditions that traditional static models fail to capture. Third, real-world scenarios frequently deviate significantly from controlled training environments, exposing the limitations of existing methods in achieving out-of-distribution generalization when faced with unseen conditions. Lastly, the lack of explicit optimization criteria or clear task termination signals further complicates the problem, forcing agents to dynamically infer implicit goals and adapt in highly ambiguous environments.

The ISLC problem has been approached through various methods, but many face critical limitations in real-world scenarios. Bayesian inference and information-theoretic strategies Baxter (1997) estimate source parameters using observed data, often guided by metrics like entropy reduction, but require extensive sampling, making them computationally expensive and less scalable in noisy or high-dimensional environments. Similarly, bio-inspired strategies like plume-tracing or zigzag algorithms perform well in structured settings but fail to generalize in dynamic conditions due to their reliance on reactive heuristics Hu et al. (2019).

Deep reinforcement learning (DRL) shows promise for learning policies in high-dimensional, dynamic environments but faces critical limitations when applied to ISLC problems. DRL Zhao et al. (2022); Hu et al. (2019); Park et al. (2022) relies heavily on predefined reward signals, which are often implicit, delayed, or absent in open-ended tasks like ISLC, creating a misalignment between the Goal (e.g., pinpointing the source) and the Optimization Objective (e.g., maximizing cumulative rewards). It also struggles with partial observability, requiring agents to infer hidden states, such as the source location Chen (2022), from noisy, sparse, and localized measurements. Additionally, in dynamic and evolving real-world fields, it is difficult to construct prior knowledge or assumptions to guide reasoning, as these environments are influenced by unpredictable factors like wind or interference Shi et al. (2024b). This further challenges DRL’s ability to adapt and learn effectively in nonstationary settings. Finally, reward sparsity and high uncertainty make exploration inefficient, hindering learning and convergence in complex environments .

To address these challenges, we propose a hierarchical framework, in Fig.1, that integrates Bayesian inference and reinforcement learning tailored to effectively tackle the ISLC problem in dynamic and uncertain environments. The framework is structured into two layers: the Inference Layer and

the Execution Layer. The Inference Layer combines particle filtering with attention mechanisms to identify and prioritize important belief states. The attention mechanism enhances the efficiency of the particle filter by focusing on high-relevance regions within the belief space, ensuring accurate and adaptive updates of source parameter estimations. Additionally, the particle filtering process evaluates whether the optimization goal—successfully locating and characterizing the source—has been achieved. Upon determining goal completion, a reward signal is generated to guide the optimization process, providing a clear direction and progression for the search. The Execution Layer, based on the inferred belief state and optimization objectives, focuses on optimizing exploration strategies to refine source parameter estimation. This layer provides two distinct approaches: Attention Particle Filtering Planning (ATT-PFP): A planning-based approach for systematic exploration of the belief space, suitable for scenarios requiring structured exploration. Attention Particle Filtering Reinforcement Learning (ATT-PFRL): A reinforcement learning-based approach that dynamically adapts policies, excelling in real-time, nonstationary environments.

The main contributions of this paper are as follows: (1) We propose a Hierarchical Attention-Based Inference Framework to solve the ISLC problem. The framework leverages an attention-enhanced particle filtering mechanism to improve inference efficiency and accuracy by focusing on high-relevance regions in dynamic and uncertain environments. (2) We prove the convergence of the attention-enhanced particle filter, ensuring its robustness in complex scenarios. Additionally, we develop two complementary execution strategies: ATT-PFP and ATT-PFRL (3) We conduct extensive experiments across diverse ISLC scenarios, demonstrating the framework’s superior performance in terms of accuracy, adaptability, and computational efficiency. Our results highlight the broad applicability of the framework to other dynamic field estimation problems.

2 Related work

Traditional methods for ISLC typically fall into two categories: Information-Theoretic Approaches and Bio-Inspired Methods. The former strategies aim to reduce uncertainty about the source location, with *Infotaxis* Vergassola et al. (2007) minimizing posterior variance, *Entrotaxis* Hutchinson et al. (2018) focusing on high-entropy regions, and *DCEE* Chen et al. (2021) balancing exploration and exploitation through uncertainty-driven decision-making. Although these methods have proven effective in controlled settings, they often rely on strong assumptions, leading to reduced efficiency and success rates when conditions deviate from their underlying assumptions. Meanwhile, the latter algorithms like *plume-tracing* Farrell et al. (2005); Wang & Pang (2022) and *zigzag* Balkovsky & Shraiman (2002); Lochmatter et al. (2008) mimic the *gradient-following behaviors* used by insects and animals—detecting changes in chemical concentration and adjusting movement to reacquire the plume if it is lost. Though effective in stable environments, these reactive approaches often fail or converge slowly in nonstationary, noisy, or complex fields, where their assumptions and simple local cues become inadequate.

Unlike traditional methods, **RL** Mnih et al. (2015); Schulman et al. (2017); Lillicrap (2015) excels in high-dimensional tasks but faces two major hurdles in ISLC: sparse or implicit rewards, where locating a hidden source offers little immediate feedback, and inference, as RL inherently lacks the capacity to directly deduce hidden variables in noisy, evolving fields. Recent efforts combine RL with Bayesian updates to address this, but many approaches still rely on hand-crafted rewards or are domain-specific. PC-DQN Zhao et al. (2022) combines particle clustering and deep Q-networks for feature extraction, demonstrating high success rates in turbulent environments. LSTM-based RL Hu et al. (2019) enhances historical trajectory encoding for robust plume tracing under dynamic conditions, while DDPG with GMM Park et al. (2022) features facilitates real-time, efficient source estimation in stochastic scenarios. Among these methods, AGDC Shi et al. (2024b) excels in handling sparse-feedback settings by detecting and halting upon goal completion while leveraging inference to improve decision-making under uncertainty. Its three variants extend its functionality: AGDC-KLD minimizes KL divergence for accurate localization Filippi et al. (2010), AGDC-ENT focuses on high-uncertainty areas Haarnoja et al. (2018), and AGDC-EE balances exploration and exploitation Li et al. (2022). Despite its advancements, AGDC still faces challenges in efficiency, particularly in inference speed and scalability, for dynamic real-time environments.

3 Preliminaries

3.1 Unified Mathematical Framework for Field Model Based on the Convection-Diffusion Equation

Many seemingly disparate natural phenomena, such as *pollutant dispersion*, *gas diffusion*, and *electric field distributions*, share common physical mechanisms: **diffusion**, **convection**, and **external sources**. These mechanisms can be described using the *convection-diffusion equation* (CDE) Holley (1969), which serves as a versatile mathematical framework:

$$\alpha \nabla^2 \phi - \vec{v} \cdot \nabla \phi + \gamma \phi + S(x, y) = 0 \quad (1)$$

where $\phi(x, y)$ represents the field variable (e.g., concentration or temperature), with $\alpha \nabla^2 \phi$, $-\vec{v} \cdot \nabla \phi$, and $S(x, y)$ accounting for diffusion, convection, and external sources, respectively. By tuning parameters such as the diffusion coefficient α , velocity \vec{v} , and source term $S(x, y)$, the CDE can describe various field phenomena, from heat conduction to pollutant transport.

3.2 Gaussian Plume Model

The Gaussian plume model, shown in Fig. 2, derived from the Convection-Diffusion Equation, leverages steady-state solutions to balance simplicity and computational efficiency. The model is analytically described by:

$$\phi(x, y) = \frac{q_s}{4\pi\psi r} \exp\left(-\frac{r}{\lambda} - \frac{(x-x_0)u_x + (y-y_0)u_y}{2\psi}\right),$$

where q_s is the source strength, r is the radial distance, u_x, u_y are convection velocities, λ is a decay parameter, and ψ is the diffusion coefficient.

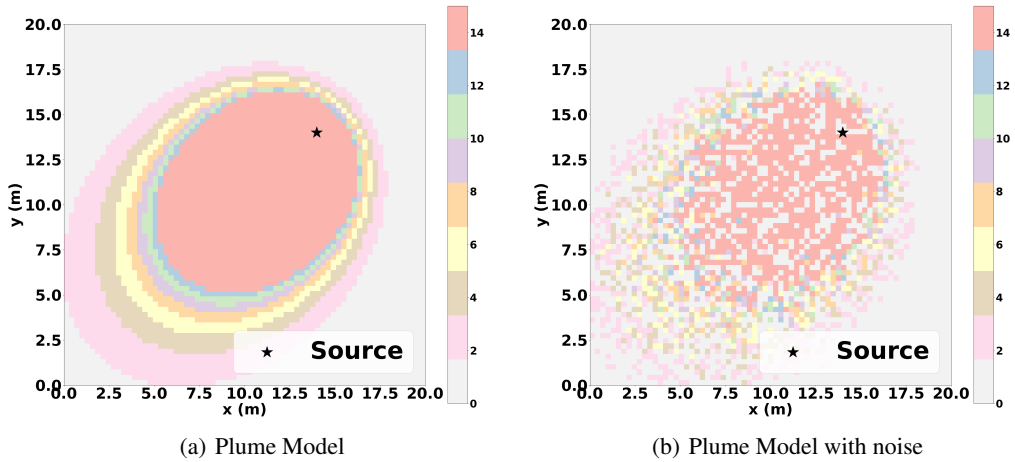


Figure 2: Gaussian Plume Model Visualisation

3.3 Partially Observable Markov Decision Process

Dynamic field modeling often involves uncertainties in observations or incomplete knowledge of the system's state. To address this, the problem can be formulated as a Partially Observable Markov Decision Process (POMDP), a probabilistic framework for decision-making under uncertainty. A POMDP is defined as a 7-tuple $(S, \Omega, A, T, Pr, R, \gamma)$, where S is the state set, A is the action set, T is the state transition probabilities, R is the reward function, Ω is the observation set, O is the observation probability function, and $\gamma \in (0, 1]$ is the discount factor. At each time step, the agent receives an observation $o_t \in \Omega$, depending on the current state and the action taken at the previous time step via the conditional observation probability $O(o_t | s_t, a_{t-1})$. By executing an action $a_t \in A$, the environment transitions to a new state according to the state transition probability $T(s_{t+1} | s_t, a_t)$,

and the agent receives a reward $r_{t+1} = R(s_t, a_t, s_{t+1})$. The goal of the agent in a POMDP is to learn an optimal policy π^* to maximize the expected future discounted sum of rewards from each time step: $R_t = E[\sum_{k=0}^{\infty} \gamma^k r_{t+k+1}]$, where the policy might be a function of the history or belief state due to the partial observability of the environment.

3.4 Sequential Importance Sampling Convergence Theorem

To ensure robust estimation in partially observable systems, the convergence of Sequential Importance Sampling (SIS) is established. The following theorem guarantees that the SIS approximation converges to the true posterior distribution as the number of particles increases.

Theorem 3.1 (Convergence of Standard SIS Doucet et al. (2001); Doucet & Johansen (2009)). *Let Θ_k represent the latent state at time k , and let $o_{1:k} = \{o_1, \dots, o_k\}$ denote the sequence of observations. Assume a Bayesian model:*

$$p(\Theta_k | o_{1:k}) \propto p(o_{1:k} | \Theta_k) p(\Theta_k), \quad (2)$$

where $p(\Theta_k)$ is the prior and $p(o_{1:k} | \Theta_k)$ the likelihood. Let $\hat{p}_N^{(SIS)}(\Theta_k | o_{1:k})$ be the particle-based approximation of the posterior. Then, under standard assumptions (e.g., bounded likelihood, consistent proposal distribution),

$$\|\hat{p}_N^{(SIS)}(\Theta_k | o_{1:k}) - p(\Theta_k | o_{1:k})\| \rightarrow 0, \quad \text{as } N \rightarrow \infty. \quad (3)$$

4 Methodology

Inverse Source Localization and Characterization under partial observability requires incorporating uncertain or unobservable state components into decision-making. To address this, We propose a methodology that combines Attention Bayesian Inference (via particle filtering) and reinforcement learning (RL) to sequentially update a belief distribution over source parameters (e.g., leak location, emission rate). The incorporation of attention mechanisms allows the model to focus on the most relevant observational data, enhancing both the accuracy and efficiency of belief updates. This approach addresses the challenges of partial observability by enabling adaptive estimation, where new observations iteratively refine the understanding of the source, bridging theoretical principles with practical application.

4.1 Bayesian Approximation for Belief Distribution

The ISLC challenge can be characterized as a **Partially Observable Markov Decision Process (POMDP)**, indicating that optimal decisions must not rely solely on immediate observations due to incomplete state information. Here, we integrate **reinforcement learning** and **Bayesian inference** to estimate the environmental dynamics—i.e., the **belief distribution**—and thereby incorporate additional unobservable information into the decision-making process.

Particle Filter for Iterative Distribution Approximation. We employ a particle filter to *iteratively approximate* the *environmental dynamics distribution*—i.e., the belief state—over time. At each time step k , this approximation is maintained via a collection of N particles, $\{\Theta_k^i, w_k^i\}_{i=1:N}$, where Θ_k^i represents the i -th point estimate of the source parameters (e.g., leak location, release rate), and w_k^i is the corresponding **importance weight**, satisfying $\sum_{i=1}^N w_k^i = 1$. Hence, the belief distribution at time k is given by

$$b(\Theta_k) = \sum_{i=1}^N w_k^i \delta(\Theta_k - \Theta_k^i), \quad (4)$$

where $\delta(\cdot)$ denotes the Dirac delta function.

Sequential Importance Sampling (SIS). The particle weights $\{w_k^i\}_{i=1:N}$ are updated following the framework of SIS Doucet et al. (2001). Specifically, we aim to approximate the posterior

$$p(\Theta_{k+1} | o_{1:k+1}) \propto p(o_{k+1} | \Theta_{k+1}) p(\Theta_{k+1} | \Theta_k) p(\Theta_k | o_{1:k}).$$

In practice, new samples $\{\Theta_{k+1}^i\}_{i=1:N}$ are drawn from a **proposal distribution** $q(\Theta_{k+1}^i \mid \Theta_k^i, \mathbf{o}_{1:k+1})$. The **unnormalized weight** \bar{w}_{k+1}^i is updated via:

$$\bar{w}_{k+1}^i \propto w_k^i \times \frac{O(o_{k+1} \mid \Theta_{k+1}^i) T(\Theta_{k+1}^i \mid \Theta_k^i)}{q(\Theta_{k+1}^i \mid \Theta_k^i, \mathbf{o}_{1:k+1})}, \quad (5)$$

where $O(o_{k+1} \mid \Theta_{k+1}^i)$ is the likelihood of observing o_{k+1} under the proposed parameters Θ_{k+1}^i , and $T(\Theta_{k+1}^i \mid \Theta_k^i)$ is the state transition model for the parameters. Dividing by $q(\Theta_{k+1}^i \mid \Theta_k^i, \mathbf{o}_{1:k+1})$ accounts for the difference between the true posterior and the proposal distribution.

Simplification under Fixed Parameters. In many ISLC scenarios, the source parameters Θ (e.g., location, emission rate) remain fixed in time. Consequently, we often adopt

$$\Theta_{k+1}^i = \Theta_k^i \quad \text{for each particle } i,$$

and choose $q(\Theta_{k+1}^i \mid \Theta_k^i, \mathbf{o}_{1:k+1}) \approx T(\Theta_{k+1}^i \mid \Theta_k^i)$. Under this assumption, $T(\Theta_{k+1}^i \mid \Theta_k^i) \approx 1$, so (5) simplifies to:

$$\bar{w}_{k+1}^i = w_k^i \cdot O(o_{k+1} \mid \Theta_{k+1}^i). \quad (6)$$

Afterwards, weights are normalized:

$$w_{k+1}^i = \frac{\bar{w}_{k+1}^i}{\sum_{j=1}^N \bar{w}_{k+1}^j}, \quad (7)$$

yielding the posterior approximation.

Convergence Properties. Recall that in Section 3 (see Theorem 3.1), we established that *standard SIS-based particle filters* converge to the true posterior distribution under mild assumptions on the likelihood, transition model, and proposal distribution. Specifically, Theorem 3.1 states that if $q(\Theta_{k+1} \mid \Theta_k, \mathbf{o}_{1:k+1})$ covers the support of the true posterior and the likelihood is well-defined, then

$$\lim_{N \rightarrow \infty} \left\| \hat{p}_N(\Theta_k \mid \mathbf{o}_{1:k}) - p(\Theta_k \mid \mathbf{o}_{1:k}) \right\| = 0, \quad ,$$

where $\|\cdot\|$ denotes an appropriate distance measure (e.g., total variation or Wasserstein).

Building on this result from Theorem 3.1, we emphasize the key role of **resampling** in mitigating weight *degeneracy*—an issue where only a small fraction of particles carry significant weights. Resampling discards negligible-weight particles and replicates high-weight ones, preserving population diversity Doucet et al. (2001); Doucet & Johansen (2009). In addition, **MCMC-based move steps** help enhance exploration by probabilistically perturbing cloned particles in accordance with the posterior. As a result, these combined strategies ensure that the particle filter remains both *stable* and *convergent*, even in noisy ISLC scenarios with partial observability, provided that the mild assumptions enumerated in Theorem 3.1 are satisfied and the number of particles N is sufficiently large.

4.2 MCMC Process with Attention Mechanism

The MCMC particle filtering framework enhanced with an attention mechanism leverages interconnected mathematical components to achieve robust and efficient state estimation. This process is grounded in probability theory, matrix analysis, and optimization techniques, allowing for effective handling of high-dimensional and uncertain environments.

Effective Sample Size (ESS) and Resampling The MCMC process begins by evaluating the uniformity of particle weights using the Effective Sample Size (ESS), calculated by:

$$\text{ESS} = \frac{\left(\sum_{i=1}^N w_i \right)^2}{\sum_{i=1}^N w_i^2},$$

where w_i denotes the weight of the i -th particle. Low ESS values indicate that a few particles dominate the weight distribution, signaling the need for resampling. This step is crucial for maintaining the diversity of the particle set and ensuring that updates remain representative of the underlying state space dynamics.

Attention-Driven Weight Refinement with MCMC Move Step After resampling, the MCMC move step employs an attention mechanism to refine particle weights by assessing their relevance to the current state estimation. The attention mechanism operates as follows:

$$\text{Attention}(\mathbf{Q}, \mathbf{K}, \mathbf{V}) = \text{softmax} \left(\frac{\mathbf{Q}\mathbf{K}^T}{\sqrt{d_k}} \right) \mathbf{V},$$

where $\mathbf{Q}, \mathbf{K}, \mathbf{V}$ act as the queries, keys, and values, respectively, with d_k representing the dimensionality of these elements. The weights $\{w_k^i\}$ are treated as the queries \mathbf{Q} , keys \mathbf{K} and values \mathbf{V} , thereby allowing each particle's weight to be recalibrated in relation to all others. This mechanism not only addresses particle degeneracy by rebalancing the weights but also captures both global and local interactions among particles, leading to a more robust tracking of the true distribution under conditions of noise and partial observability.

Covariance Matrix and Particle Perturbation With weights refined, the procedure calculates the weighted covariance matrix, Σ , which quantifies the uncertainty and spread of the belief across the distribution of belief states Θ :

$$\Sigma = \mathbb{E}_w [\Theta\Theta^T] - \mathbb{E}_w[\Theta]\mathbb{E}_w[\Theta]^T,$$

where $\mathbb{E}_w[\cdot]$ represents the expectation calculated with weights adjusting each particle's contribution. Regularization is applied to the covariance matrix by adding a small positive constant to its diagonal ($\Sigma + \epsilon\mathbf{I}$), ensuring numerical stability and positive definiteness for the subsequent Cholesky decomposition, $\mathbf{L} = \text{Cholesky}(\Sigma)$. This decomposition transforms the covariance matrix into a lower triangular matrix \mathbf{L} , which facilitates the efficient sampling of new particle states from multivariate Gaussian distributions, crucial for effectively exploring the state space.

State Updates and Log-Likelihood Ratio Particle states are updated using the formula:

$$\Theta_{new} = \Theta + h_{opt}\Sigma^{1/2}\xi,$$

where h_{opt} represents the optimal bandwidth for perturbation, calculated to balance exploration and the focusing on high-probability regions, and $\xi \sim \mathcal{N}(0, \mathbf{I})$ denotes Gaussian noise. The viability of these states is assessed using a log-likelihood ratio, which compares the plausibility of transitioning from the current state to the proposed state, emphasizing states that minimize deviations from expected dynamics.

Acceptance Ratio and System State Estimation The acceptance of new states into the particle set is governed by an acceptance ratio (β), formulated as:

$$\beta = \frac{p(\Theta_{new})}{p(\Theta)} \cdot \exp \left(-\frac{1}{2} [\Delta_{new}^T \Sigma^{-1} \Delta_{new} - \Delta_{old}^T \Sigma^{-1} \Delta_{old}] \right),$$

where Δ_{new} and Δ_{old} represent the deviations of the new and old belief states from their respective means, adjusted for the covariance matrix Σ . This measure, often referred to as the logratio, quantifies the transition plausibility by comparing the probability densities of the new and current states under the model's assumptions.

This detailed explanation emphasizes the sophisticated interplay of mathematical principles that underpin the MCMC process with an attention mechanism, ensuring thorough understanding and implementation fidelity in practical scenarios.

4.3 Cessation Mechanism

Particle filters estimate state distributions in unknown environments by refining state representations using observational data. A key feature of these models is their ability to terminate operations autonomously based on statistical criteria, improving computational efficiency. Specifically, the process ceases when the standard deviation (STD) of the belief states (Θ_k) falls below a predefined threshold (ζ), indicating convergence. The STD is calculated as:

$$STD = \sqrt{\text{diag}(E[(\Theta - E[\Theta])^2])},$$

Table 1: Parameter Distributions for the Training Scenarios

Source Parameter	Distribution
location of field source x_s	Uniform $\mathcal{U}(5, 20)$
location of field source y_s	Uniform $\mathcal{U}(10, 20)$
Release Strength q_s	Uniform $\mathcal{U}(10, 3000)$
Wind Speed u_x, u_y	Uniform $\mathcal{U}(0, 6)$
Decay parameter λ	Uniform $\mathcal{U}(0, 8)$
Diffusivity ψ	Uniform $\mathcal{U}(1, 5)$
Sensor Noise ϵ	Fixed at 0.5
Environmental Noise σ	Fixed at 0.4
Effective Samples N_{eff}	Fixed at 0.6

where $diag(\cdot)$ extracts the variances of each state dimension. When $STD < \zeta$, the particle states are considered sufficiently precise, and further computation becomes redundant. At this point, a non-zero reward guides the execution layer to achieve the predefined accuracy threshold. This mechanism ensures efficient resource use and reinforces the optimization strategy, while also supporting adaptive behavior in dynamic environments.

Table 2: Comparison of REV Metric Across Different Scenarios

Method Group	REV Range (Mean \pm Std)
ATT-PFRL (ours)	0.12–0.15 \pm 0.07
AGDC (KLD, ENT, EE)	0.09–0.10 \pm 0.05
ATT-PFP, Infotaxis	1.2–1.6 \pm 0.08
Entrotaxis, DCEE	1.1–1.4 \pm 0.07
Random	< 0.01

4.4 Integration of RL and planning in POMDPs

In POMDPs, decision-making under uncertainty is achieved by integrating probabilistic belief states $b(\Theta_k)$ with real-time observations o_k . The state $s_k = (b(\Theta_k), o_k)$ combines the predictive capabilities of the belief state with the immediate context provided by observations, enabling adaptive and robust strategies for complex tasks like source localization. Based on this enhanced state representation, we propose two approaches: *Attention Particle Filtering Planning (Att-PFP)* and *Attention Particle Filtering RL (Att-PFRL)*.

Att-PFP aims to maximize the cumulative reward over a finite horizon: $\max \sum_{t=0}^T \gamma^t R_t$, where T is the planning horizon. This approach leverages a planning process guided by an attention mechanism, which focuses on high-value regions in the belief distribution, improving computational efficiency and precision in uncertainty reduction. In contrast, *Att-PFRL* optimizes a policy $\pi_\theta(s_k)$ through reinforcement learning to maximize the expected cumulative reward over an infinite horizon: $\max_{\pi_\theta} E[\sum_{t=0}^{\infty} \gamma^t R_t]$. An attention mechanism is used to refine noisy observations and enhance the learning process. The policy is improved iteratively by updating the value function $V(s_k)$ based on the temporal difference (TD) error: $\delta_k = r_{k+1} + \gamma V(s_{k+1}) - V(s_k)$, and $V(s_k)$ is adjusted as $V(s_k) \leftarrow V(s_k) + \alpha \delta_k$, where α is the learning rate.

5 Experiments

In this paper, we utilized the ISLC environments (ISLCenv) to investigate source localization in various scenarios. The STE environment, described in the Appendix or (Shi et al. (2024a)), includes a Gaussian model to simulate the field distribution from multiple sources and a sensor model to capture intensity readings. Instead of directly rewarding the agent, the environment provides positional and intensity observations at each step, requiring RL algorithms to adapt their strategies for effective source localization across diverse environmental conditions.

Table 3: Comparison of Baseline Methods Under Different Scenarios (OCE, ADE, LPS)

Metric	Method	Temp.	Conc.	Mag.	Elec.	Gas	En.	Noise
OCE	ATT-PFRL(ours)	0.95±0.05	0.94±0.05	0.94±0.05	0.82±0.04	0.96±0.05	0.63±0.03	0.94±0.05
	AGDC-KLD	0.90±0.05	0.91±0.05	0.89±0.04	0.77±0.04	0.92±0.05	0.61±0.03	0.91±0.05
	AGDC-ENT	0.80±0.04	0.81±0.04	0.81±0.04	0.68±0.03	0.79±0.04	0.51±0.03	0.80±0.04
	AGDC-EE	0.87±0.04	0.88±0.04	0.86±0.04	0.74±0.04	0.86±0.04	0.57±0.03	0.86±0.04
	ATT-PFP(ours)	0.90±0.05	0.91±0.05	0.89±0.04	0.73±0.04	0.89±0.04	0.57±0.03	0.89±0.04
	Infotaxis	0.85±0.04	0.86±0.04	0.85±0.04	0.75±0.04	0.84±0.04	0.55±0.03	0.80±0.04
	Entrotaxis	0.24±0.01	0.23±0.01	0.25±0.01	0.15±0.01	0.22±0.01	0.14±0.01	0.23±0.01
	DCEE	0.58±0.03	0.59±0.03	0.58±0.03	0.43±0.02	0.56±0.03	0.36±0.02	0.57±0.03
	Random	< 0.5	< 0.05	< 0.05	< 0.05	< 0.05	< 0.05	< 0.05
ADE	ATT-PFRL(ours)	20±1.0	19±1.0	18±0.9	19±0.8	17±0.9	19±0.5	19±1.0
	AGDC-KLD	23±1.2	22±1.1	22±1.1	23±0.9	20±1.0	22±0.6	21±1.1
	AGDC-ENT	25±1.3	24±1.2	25±1.2	20±1.0	22±1.1	24±0.7	23±1.2
	AGDC-EE	25±1.3	24±1.2	24±1.2	19±1.0	21±1.1	23±0.7	22±1.1
	ATT-PFP(ours)	45±2.3	43±2.2	42±2.1	44±1.8	40±2.0	45±1.3	42±2.1
	Infotaxis	50±2.5	48±2.4	51±2.4	58±1.9	43±2.2	47±1.4	45±2.3
	Entrotaxis	62±3.1	60±3.0	59±3.0	61±2.5	56±2.8	55±1.8	58±2.9
	DCEE	57±2.9	55±2.8	54±2.7	55±2.3	51±2.6	57±1.6	53±2.7
	Random	> 150	> 150	> 150	> 150	> 150	> 150	> 150
LPS	ATT-PFRL(ours)	0.05±0.01	0.05±0.01	0.05±0.01	0.08±0.01	0.05±0.01	0.06±0.01	0.05±0.01
	AGDC-KLD	0.2 ±0.01	0.2 ±0.01	0.2 ±0.01	0.17±0.01	0.2 ±0.01	0.13±0.01	0.2 ±0.01
	AGDC-ENT	0.25±0.01	0.24±0.01	0.24±0.01	0.20±0.01	0.22±0.01	0.14±0.01	0.23±0.01
	AGDC-EE	0.23±0.01	0.22±0.01	0.22±0.01	0.18±0.01	0.20±0.01	0.12±0.01	0.21±0.01
	ATT-PFP(ours)	0.25±0.01	0.24±0.01	0.23±0.01	0.19±0.01	0.21±0.01	0.13±0.01	0.22±0.01
	Infotaxis	0.6 ±0.03	0.6 ±0.03	0.6 ±0.03	0.51±0.02	0.6 ±0.03	0.39±0.02	0.6 ±0.03
	Entrotaxis	0.7 ±0.04	0.7 ±0.04	0.7 ±0.04	0.60±0.03	0.7 ±0.04	0.46±0.02	0.7 ±0.04
	DCEE	0.6 ±0.03	0.6 ±0.03	0.6 ±0.03	0.51±0.02	0.6 ±0.03	0.39±0.02	0.6 ±0.03
	Random	5.0 ±0.25	4.7 ±0.24	4.5 ±0.23	3.8 ±0.19	4.3 ±0.22	2.8 ±0.14	4.3 ±0.22

5.1 Baseline Algorithms and Evaluation Metrics

The performance of the proposed and baseline algorithms is evaluated using four metrics: *Operational Completion Efficacy (OCE)* measures the frequency with which emergency response missions achieve their objectives, with higher values reflecting effective deployment strategies. *Average Deployment Efficiency (ADE)* captures the average distance traveled by response units, where lower values indicate more direct and efficient routing. *Response Execution Velocity (REV)* quantifies the total time taken from deployment to mission completion, with faster execution highlighting efficient operations. Finally, *Localization Precision Score (LPS)* assesses the accuracy of source localization by measuring the average deviation between estimated and actual source locations, with lower values indicating higher precision.

To evaluate performance against these metrics, we compare our approach to several baseline algorithms. We categorize these baselines into two groups based on their methodological frameworks. The first group combines reinforcement learning with Bayesian inference, including *AGDC* Shi et al. (2024b) and its variants—*AGDC-KLD*, *AGDC-ENT*, and *AGDC-EE*. The second group integrates planning with Bayesian inference, represented by *Infotaxis* Vergassola et al. (2007), *Entrotaxis* Hutchinson et al. (2018), and *DCEE* Chen et al. (2021). This classification aids in clarifying the impact of different inferential strategies on performance in environments characterized by sparse feedback. A *Random* baseline serves to provide a foundational comparison, underscoring the advantages of informed decision-making.

The experiments were conducted across multiple types of fields, including *Temperature (Temp.)*, *Concentration (Conc.)*, *Magnetic (Mag.)*, *Electric (Elec.)*, *Gas (Gas)*, *Energy (En.)*, and *Noise (Noise)*, representing diverse environmental conditions for source localization tasks. Each field type poses unique challenges in terms of signal characteristics and environmental dynamics, providing a comprehensive evaluation platform for the algorithms.

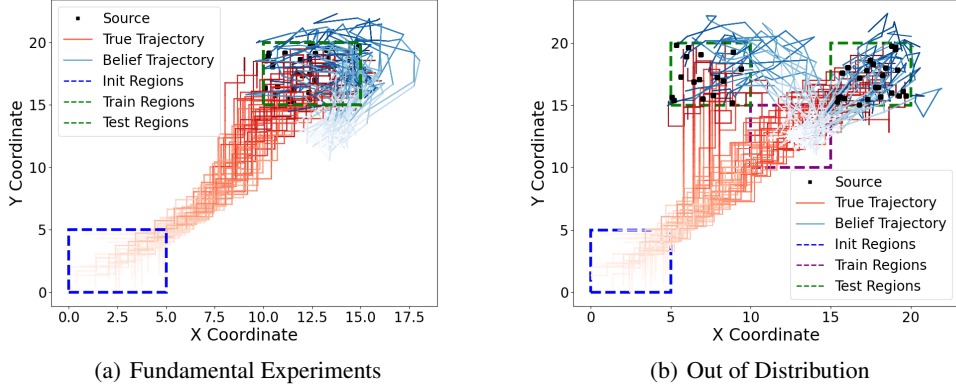


Figure 3: Design of Experiments

5.2 Scenario Parameterization and Evaluation

The training scenarios, defined within a 20×20 area as fundamental experiments, are generated by randomly initializing the source and environmental parameters at the start of each episode, including the gas source location, wind speed, and wind direction, sampled from the probability distributions in Table 1. The agent begins its search from a random position within the $(0, 5) \times (0, 5)$ region, moving at a speed of 1 meter per step to ensure exposure to a diverse range of scenarios, facilitating robust learning. The testing scenarios comprise 1,000 randomly generated conditions distinct from the training data. While drawn from the same parameter ranges, these scenarios introduce new specific conditions to evaluate the model’s performance on unseen data.

For the study on experiments in out-of-distribution scenarios, the training region is confined to $(10, 15) \times (10, 15)$, while the testing regions are defined as $(5, 10) \times (15, 20)$ and $(15, 20) \times (15, 20)$. This setup ensures that the testing conditions differ spatially from the training region, providing a robust evaluation of the model’s generalization ability beyond the distribution of the training data.

5.3 Fundamental Experiments

In the fundamental experiments, our methods (ATT-PFRL and ATT-PFP) showcase not only superior performance across various environmental conditions but also illustrate the benefit of robust algorithm design in Table 3 and 2. ATT-PFRL, for instance, consistently exhibits high OCE scores, such as 0.95 ± 0.05 in Temperature and 0.96 ± 0.05 in Gas, which demonstrates its effectiveness in completing missions under diverse conditions. Compared to other methods, such as AGDC-KLD and AGDC-EE, which show lower OCE scores (e.g., 0.90 ± 0.05 and 0.87 ± 0.04 respectively in Temperature), our methods prove to be more reliable. The ADE metric further accentuates this point, with ATT-PFRL maintaining lower values (e.g., 20 ± 1.0 in Temperature), suggesting more efficient navigation compared to DCEE and Entrotaxis, whose ADE exceeds 50 ± 2.5 in challenging fields.

5.4 Out of Distribution Problem

The Out-of-Distribution (OOD) experiments, summarized in the left part of the Fig 4, highlight the robustness of our method, ATT-PFRL, in handling unseen scenarios. ATT-PFRL achieves the highest OCE values across all fields, such as 0.95 in the Temperature field and 0.96 in the Gas field, demonstrating superior generalization capabilities. It also maintains low ADE values (e.g., 20 in Temperature and 17 in Gas), indicating efficient navigation, and stable LPS values (e.g., 0.15 in Temperature), showcasing precise source localization. In contrast, baseline methods exhibit significant performance gaps. For example, AGDC-KLD achieves moderate OCE scores (e.g., 0.448 in Temperature) but suffers from higher ADE (e.g., 23 in Temperature). AGDC-Entropy and AGDC-EE show even lower OCE (e.g., 0.271 and 0.288 in Temperature) and less efficient navigation (ADE of 25). The Energy field emerges as the most challenging, where ATT-PFRL achieves a reduced OCE of 0.63, yet still outperforms baseline methods such as AGDC-KLD (OCE 0.307) and AGDC-Entropy

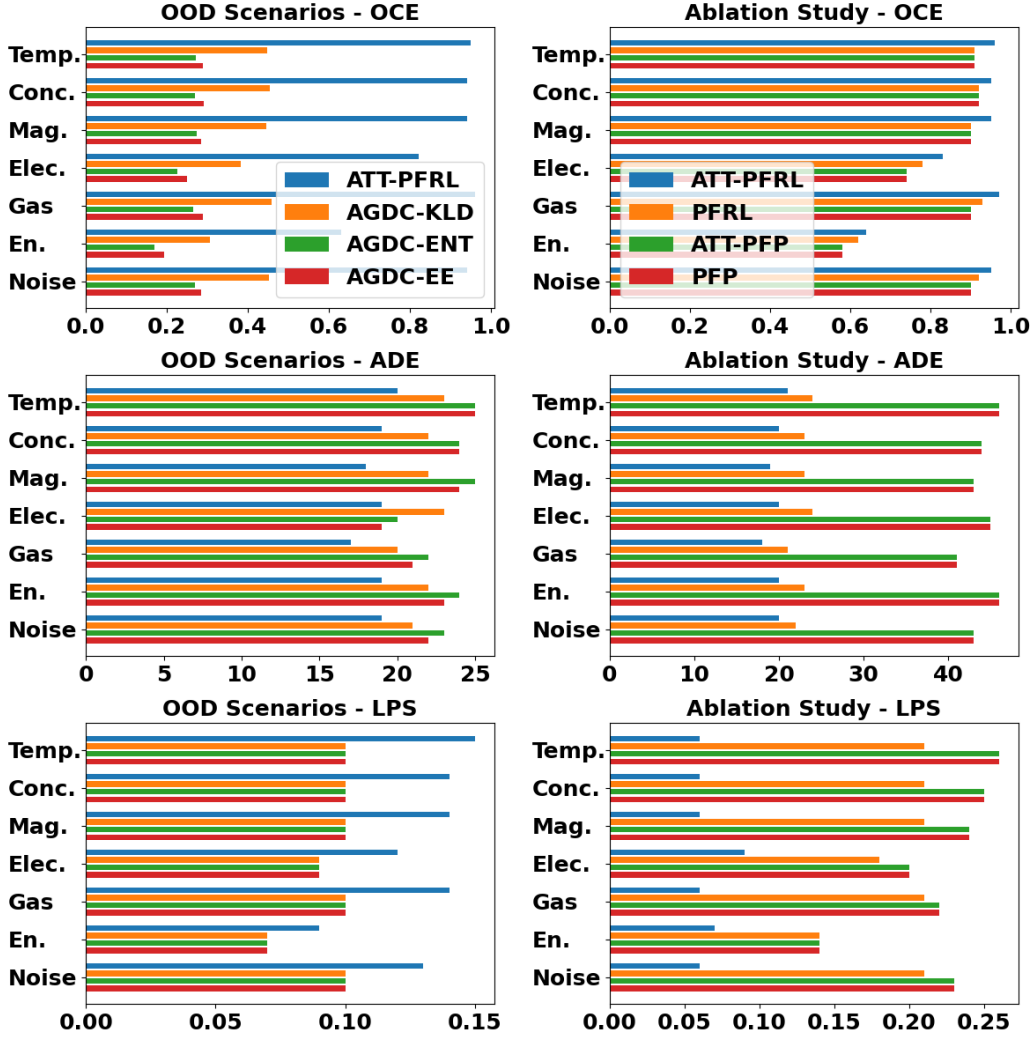


Figure 4: Out of Distribution (left) and ablation study(right)

(OCE 0.168). These results emphasize ATT-PFRL’s adaptability and efficiency in complex, dynamic environments while exposing the limitations of the baseline methods under OOD conditions.

5.5 Ablation Experiment

The ablation study distinctly demonstrates the significant role of the attention mechanism in enhancing algorithm performance in the left part of the Fig 4. By comparing ATT-PFRL and ATT-PFP against their counterparts without attention (PFRL and PFP), we see notable improvements in both OCE and LPS metrics. For example, ATT-PFRL in the Temperature field records an LPS of 0.06, markedly lower than PFRL’s 0.21, highlighting the precision gained through the integration of attention. Such findings validate the attention mechanism’s capacity to refine decision-making and adaptability, particularly in environments requiring high levels of accuracy and operational efficacy.

6 Conclusion

In this paper, we presented a novel hierarchical framework to address the challenges of the ISLC problem in dynamic and uncertain environments. By integrating Bayesian inference with reinforcement learning, and enhancing particle filtering through an attention mechanism, our framework achieves

efficient and accurate estimation of source parameters. The two execution strategies, Att-PFP and Att-PFRL, cater to structured exploration and real-time decision-making, respectively, providing flexibility in various scenarios. Theoretical guarantees ensure the convergence of the attention-enhanced particle filter, while empirical results demonstrate the framework's superior performance across diverse ISLC scenarios, including out-of-distribution cases. This work not only advances the state-of-the-art in ISLC but also lays the foundation for future research in dynamic field estimation and adaptive decision-making in uncertain environments.

References

- Balkovsky, E. and Shraiman, B. I. Olfactory search at high reynolds number. *Proceedings of the national academy of sciences*, 99(20):12589–12593, 2002.
- Baxter, J. A bayesian/information theoretic model of learning to learn via multiple task sampling. *Machine learning*, 28:7–39, 1997.
- Chen, W.-H. Perspective view of autonomous control in unknown environment: Dual control for exploitation and exploration vs reinforcement learning. *Neurocomputing*, 497:50–63, 2022.
- Chen, W.-H., Rhodes, C., and Liu, C. Dual control for exploitation and exploration (dcee) in autonomous search. *Automatica*, 133:109851, 2021.
- Doucet, A. and Johansen, A. M. A tutorial on particle filtering and smoothing: Fifteen years later. In Crisan, D. and Rozovski, B. (eds.), *Handbook of Nonlinear Filtering*, pp. 656–704. Oxford University Press, Oxford, UK, 2009.
- Doucet, A., de Freitas, N., and Gordon, N. (eds.). *Sequential Monte Carlo Methods in Practice*. Springer, New York, NY, USA, 2001.
- Farrell, J. A., Pang, S., and Li, W. Chemical plume tracing via an autonomous underwater vehicle. *IEEE Journal of Oceanic Engineering*, 30(2):428–442, 2005.
- Filippi, S., Cappé, O., and Garivier, A. Optimism in reinforcement learning and kullback-leibler divergence. In *2010 48th Annual Allerton Conference on Communication, Control, and Computing (Allerton)*, pp. 115–122. IEEE, 2010.
- Haarnoja, T., Zhou, A., Abbeel, P., and Levine, S. Soft actor-critic: Off-policy maximum entropy deep reinforcement learning with a stochastic actor. In *International conference on machine learning*, pp. 1861–1870. PMLR, 2018.
- Holley, E. R. Unified view of diffusion and dispersion. *Journal of the Hydraulics division*, 95(2): 621–632, 1969.
- Hu, H., Song, S., and Chen, C. P. Plume tracing via model-free reinforcement learning method. *IEEE transactions on neural networks and learning systems*, 30(8):2515–2527, 2019.
- Hutchinson, M., Oh, H., and Chen, W.-H. Entrotaxis as a strategy for autonomous search and source reconstruction in turbulent conditions. *Information Fusion*, 42:179–189, 2018.
- Li, Z., Chen, W.-H., and Yang, J. Concurrent active learning in autonomous airborne source search: Dual control for exploration and exploitation. *IEEE Transactions on Automatic Control*, 68(5): 3123–3130, 2022.
- Lillicrap, T. Continuous control with deep reinforcement learning. *arXiv preprint arXiv:1509.02971*, 2015.
- Lochmatter, T., Raemy, X., Matthey, L., Indra, S., and Martinoli, A. A comparison of casting and spiraling algorithms for odor source localization in laminar flow. In *2008 IEEE International Conference on Robotics and Automation*, pp. 1138–1143. IEEE, 2008.
- Mnih, V., Kavukcuoglu, K., Silver, D., Rusu, A. A., Veness, J., Bellemare, M. G., Graves, A., Riedmiller, M., Fidjeland, A. K., Ostrovski, G., et al. Human-level control through deep reinforcement learning. *nature*, 518(7540):529–533, 2015.
- Park, M., Ladosz, P., and Oh, H. Source term estimation using deep reinforcement learning with gaussian mixture model feature extraction for mobile sensors. *IEEE Robotics and Automation Letters*, 7(3):8323–8330, 2022.
- Schulman, J., Wolski, F., Dhariwal, P., Radford, A., and Klimov, O. Proximal policy optimization algorithms. *arXiv preprint arXiv:1707.06347*, 2017.
- Shi, Y., McAreavey, K., Liu, C., and Liu, W. Reinforcement learning for source location estimation: A multi-step approach. In *2024 IEEE International Conference on Industrial Technology (ICIT)*, pp. 1–8. IEEE, 2024a.

- Shi, Y., Wen, M., Zhang, Q., Zhang, W., Liu, C., and Liu, W. Autonomous goal detection and cessation in reinforcement learning: A case study on source term estimation. *arXiv preprint arXiv:2409.09541*, 2024b.
- Steiner, H. and Bushe, W. Large eddy simulation of a turbulent reacting jet with conditional source-term estimation. *Physics of Fluids*, 13(3):754–769, 2001.
- Vergassola, M., Villermaux, E., and Shraiman, B. I. ‘infotaxis’ as a strategy for searching without gradients. *Nature*, 445(7126):406–409, 2007.
- Wang, L. and Pang, S. Robotic odor source localization via adaptive bio-inspired navigation using fuzzy inference methods. *Robotics and Autonomous Systems*, 147:103914, 2022.
- Zhao, Y., Chen, B., Wang, X., Zhu, Z., Wang, Y., Cheng, G., Wang, R., Wang, R., He, M., and Liu, Y. A deep reinforcement learning based searching method for source localization. *Information Sciences*, 588:67–81, 2022.